

THE EVOLUTION OF THE UV LUMINOSITY FUNCTION FROM $Z \sim 0.75$ TO $Z \sim 2.5$ USING HST ERS
WFC3/UVIS OBSERVATIONS¹P. A. OESCH², R. J. BOUWENS^{3,4}, C. M. CAROLLO², G. D. ILLINGWORTH³, D. MAGEE³,
M. TRENTI⁵, M. STIAVELLI⁶, M. FRANX⁴, I. LABBÉ⁷, P. G. VAN DOKKUM⁸*Draft version December 1, 2010*

ABSTRACT

We present UV luminosity functions (LFs) at 1500 Å derived from the HST Early Release Science WFC3/UVIS data acquired over ~ 50 arcmin² of the GOODS-South field. The LFs are determined over the entire redshift range $z = 0.75 - 2.5$ using two methods, similar to those used at higher redshifts for Lyman Break Galaxies (LBGs): (1) 13-band UV+optical+NIR photometric redshifts to study galaxies in the range $z = 0.5 - 2$ in three bins of $dz = 0.5$, and (2) dropout samples in three redshift windows centered at $z \sim 1.5$, $z \sim 1.9$, and $z \sim 2.5$. The characteristic luminosity dims by 1.5 mag from $z = 2.5$ to $z = 0.75$, consistent with earlier work. However, the other Schechter function parameters, the faint-end slope and the number density, are found to be remarkably constant over the range $z = 0.75 - 2.5$. Using these LF determinations we find the UV luminosity density to increase by ~ 1.4 dex according to $(1+z)^{2.58 \pm 0.15}$ from $z \sim 0$ to its peak at $z \sim 2.5$. Strikingly, the inferred faint-end slopes for our LFs are all steeper than $\alpha = -1.5$, in agreement with higher-redshift LBG studies. Since the faint-end slope in the local universe is found to be much flatter with $\alpha \simeq -1.2$, this poses the question as to when and how the expected flattening occurs. Despite relatively large uncertainties, our data suggest $\alpha \simeq -1.7$ at least down to $z \sim 1$. These new results from such a shallow early dataset demonstrate very clearly the remarkable potential of WFC3/UVIS for the thorough characterization of galaxy evolution over the full redshift range $z \sim 0.5$ to $z \sim 3$.

Subject headings: galaxies: evolution — galaxies: high-redshift — galaxies: luminosity function, mass function

1. INTRODUCTION

The UV Luminosity Function (LF) of galaxies is a key diagnostic for establishing the contributions of galaxies of different luminosities and masses to the cosmic star-formation rate (SFR) density. In addition, in combination with other measures, like the galaxy mass function, it also provides essential clues as to the causes for the slow down in star-formation of galaxies in more recent times since $z \sim 2$.

The UV LF has been studied very extensively at redshifts $2 \lesssim z \lesssim 6$, but at lower redshifts ($z \lesssim 2$), similar deep, high resolution data has not been available. To date the $z < 2$ UV LF has been measured from GALEX data using the dropout technique (e.g. Burgarella et al. 2006; Ly et al. 2009; Haberland et al. 2009), and also using spectroscopic or photometric redshifts (e.g. Arnouts et al. 2005; Wyder et al. 2005; Budavári et al. 2005). The main limitations of the GALEX results are (1) the very wide point-spread func-

tion (PSF; $\sim 5''$ FWHM), which may cause blending of the UV light from several sources and makes the identification of optical counterparts relatively difficult, and (2) the limited depth (~ 25 mag).

With the installation of the Wide-Field Camera 3 (WFC3) on the Hubble Space Telescope (HST), the efficient coverage of the electromagnetic spectrum at high spatial resolution ($\lesssim 0''.15$) has been extended to the UV and to the IR. The new IR capability allowed us (and other groups) to perform the first robust measurements of the UV LF at $z \sim 7 - 8$ in the first-epoch data of the HUDF09 (e.g. Oesch et al. 2010b; Bouwens et al. 2010; McLure et al. 2010; Bunker et al. 2010).

The high sensitivity UV imaging capability provided by the WFC3/UVIS channel similarly allows us to derive the UV LF at redshifts below $z \sim 2.5$, where the ~ 1500 Å UV flux from galaxies could not be probed efficiently with previous high resolution cameras. While the depth of the current ERS WFC3/UVIS UV data (Windhorst et al. 2010) is less than that of the WFC3/IR data, the present depths still significantly exceed that from any previous UV data set.

We use two different methods for our LF determinations: (1) 13-band UV+optical+NIR photometric redshifts to study galaxies in the range $z \sim 0.5 - 2$, and (2) the UV dropout technique, applied to the UVIS filter set, which allows for the selection of star-forming galaxies at $z \sim 1.3$ to $z \sim 2.8$. The latter dropout samples are similar to the recent selections of Hathi et al. (2010).

In Section 2 we describe the data, the photometric redshift estimates and the dropout selection. This is followed in Section 3 by our constraints on the UV LF be-

¹ Based on data obtained with the *Hubble Space Telescope* operated by AURA, Inc. for NASA under contract NAS5-26555.

² Institute for Astronomy, ETH Zurich, 8092 Zurich, Switzerland; poesch@phys.ethz.ch

³ UCO/Lick Observatory, University of California, Santa Cruz, CA 95064

⁴ Leiden Observatory, Leiden University, NL-2300 RA Leiden, Netherlands

⁵ University of Colorado, Center for Astrophysics and Space Astronomy, 389-UCB, Boulder, CO 80309, USA

⁶ Space Telescope Science Institute, Baltimore, MD 21218, United States

⁷ Carnegie Observatories, Pasadena, CA 91101, Hubble Fellow

⁸ Department of Astronomy, Yale University, New Haven, CT 06520

tween $z = 0.5$ – 2.8 , and we end with a short discussion on the evolution of the UV LF parameters and luminosity density in Section 4.

Throughout this letter, we adopt $\Omega_M = 0.3, \Omega_\Lambda = 0.7, H_0 = 70 \text{ kms}^{-1}\text{Mpc}^{-1}$, i.e. $h = 0.7$. Magnitudes are given in the AB system (Oke & Gunn 1983).

2. DATA AND SAMPLE SELECTION

2.1. ERS Data Set

The Early Release Science (ERS) UV data cover a total of $\sim 50 \text{ arcmin}^2$ of the GOODS-South fields (Giavalisco et al. 2004) in 4×2 pointings of WFC3/UVIS in three filters ($UV_{225} - F225W$, $UV_{275} - F275W$, $U_{336} - F336W$). Each pointing was covered with five orbits, equivalent to 2778 s, 5688 s, and 5688 s integrations in UV_{225} , UV_{275} , and U_{336} , respectively. The observations in each band were split into three (U_{336}) or four ($UV_{225/275}$) exposures to facilitate cosmic-ray (and bad pixel) removal (see Windhorst et al. 2010, for more information on the data). The RMS maps were scaled to the proper noise level, as measured in circular apertures appropriate for the galaxies under study. Using circular apertures of $0''.2$ radius, the measured 5σ point source sensitivities in all three filters are 26.8–26.9 mag.

After masking areas with bad sampling and large residuals from cosmic ray hits the final area used in this study with both ACS and WFC3/UVIS coverage is $\sim 47 \text{ arcmin}^2$.

The reduced UVIS images were registered to the GOODS ACS B-band frames (version 2; M. Giavalisco and the GOODS Team, 2010, in preparation⁹) and drizzled to the same pixel scale of $0''.03$. The most recent in-flight geometric distortion solutions (02/2010) were essential for obtaining good alignment. Sources were detected in the ACS B-band image using SExtractor (Bertin & Arnouts 1996), resulting in 6683 detections down to 28 mag. Colors were measured in dual image mode in isophotal apertures to maximize the S/N.

Lastly, our catalog was matched against the public GOODS catalogs and candidate stars flagged. At $z_{850} < 25.5$ this identification is based upon their size (half-light radii $< 0''.09$) and the SExtractor stellarity parameter (> 0.8). Faintward of 25.5, the latter parameter is no longer reliable, and therefore flagging sources with half-light radii $< 0''.09$ was done if the $V - i$ vs. $i - z$ colors of sources were consistent with the stellar sequence (within 0.15 mag). From a visual inspection of the sample of galaxies entering in the LF estimates this has proven to be a very efficient and complete procedure to identify stars.

2.2. Photometric Redshift Selections

In order to derive accurate photometric redshifts, we supplement the high resolution ACS and WFC3/UVIS data with ground-based IR and with Spitzer data, using the GOODS-MUSIC catalog (v2) of Santini et al. (2009). In particular, the GOODS-MUSIC photometry used here is VIMOS U , ACS $B_{435}/V_{606}/i_{775}/z_{850}$, ISAAC J, H, K , and Spitzer IRAC 3.6 and 4.5. The GOODS-MUSIC catalog is 90% complete down to $z_{850} \leq 26$ mag. Matching this catalog to our B-selected sources, we find 4165

matches (using a $0''.2$ error tolerance). The UVIS isophotal fluxes are scaled to total fluxes using the ratio of B-Band ISO flux to B-Band AUTO flux.

Thus, our basic photometry catalog for photo- z estimates consists of 7 filter HST data, complemented with 4 PSF-matched ground based filters, and the two shortest wavelength IRAC bands. The IRAC 5.8 and 8.0 bands were omitted, since they are dominated by dust and PAH emission for lower redshift galaxies. Even if galaxies are generally red in $B - z$, we limit our analysis to $B_{435} < 26$ mag to avoid incompleteness corrections due to the z_{850} -band limit. We did not use the WFC3/IR photometry, since it is not available for all sources to keep our analysis as uniform as possible (and our tests show that our selections do not change significantly when these data are included).

Photometric redshifts were estimated from spectral energy distribution (SED) fitting with ZEBRA (Feldmann et al. 2006). The adopted SED set is based on Bruzual & Charlot (2003) composite stellar populations. In particular, we computed 15 median templates as a function of rest-frame $u - J$ color for galaxies in the zCOSMOS survey (Lilly et al. 2007; Lilly et al. 2009). Subsequently, these templates were corrected for systematic offsets with respect to the COSMOS photometry (Capak et al. 2007) using ZEBRA, and the major emission lines ($\text{Ly}\alpha$, $\text{H}\alpha$, $\text{H}\beta$, OII , and OIII) were added using the Kennicutt (1998) relations between UV luminosity and emission line strengths. Finally, dust was added to this set of templates using the Calzetti et al. (2000) dust law with $E(B - V) = 0 - 0.5$, resulting in a final set of 2052 templates.

We used this template set to derive photometric redshifts for our combined catalog of UVIS and GOODS-MUSIC photometry. We compared our estimates with spectroscopic redshift measurements compiled in the GOODS-MUSIC catalog. From a total of 462 sources with reliable spectroscopy (363 at $z < 1.5$), we find an accuracy of $\sigma_z = 0.037 \times (1+z)$, with only 6.4% of sources having redshift errors larger than $|\Delta(z)| > 0.15 \times (1+z)$. Our photometric redshift estimates are therefore sufficiently precise to derive LFs in bins of $dz = 0.5$.

2.3. UV Dropout Selection

Most of the UV LFs at $z > 3$ are based on an LBG selection (e.g. Steidel et al. 1995). The same technique can also be applied to the WFC3/UVIS filters, allowing the selection of star-forming galaxies as UV dropouts. At $z < 3$, the Lyman break seen in galaxies is primarily the result of neutral hydrogen within the sources themselves, in significant contrast to the situation at $z > 3$, where the break is also due to Lyman-series absorption from the IGM.

Our selection criteria are based on standard color-color diagrams, which are shown in Figure 1. In particular, the selection regions are chosen to identify an unbiased sample of star-forming galaxies with dust extinction less than $E(B - V) \sim 0.3 - 0.4$ guarding against lower redshift interlopers.

Specifically, the adopted selection criteria for UV_{225} dropouts are:

$$UV_{225} - UV_{275} > 0.75 \quad \wedge \\ UV_{225} - UV_{275} > 1.67(UV_{275} - U_{336}) - 0.42 \quad \wedge$$

⁹ <http://archive.stsci.edu/pub/hlsp/goods/v2/>

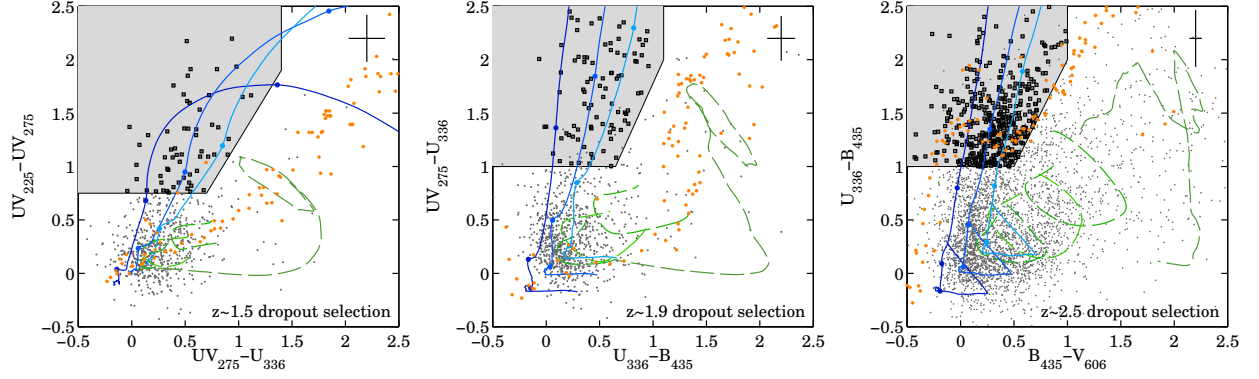


FIG. 1.— The color selection of UV-dropouts at redshifts $z \sim 1.5$, 1.9 , and 2.5 (from left to right). Blue lines represent tracks of star-forming galaxies with dust obscuration of $E(B-V) = 0, 0.15, 0.3$. The green dashed lines are the expected colors of lower redshift galaxies (Coleman et al. 1980). These tracks extend to $z < 1.1$, $z < 1.5$, and $z < 2$ for the different figures respectively. The gray shaded regions are the adopted selection regions for dropout galaxies. The orange points are stars from the Pickles (1998) library. Stars are removed from our samples using a combination of the stellarity parameter and $(V-i)$ vs. $(i-z)$ colors, as described in the text. The light gray dots represent all galaxies in the catalog down to the respective magnitude limits adopted in our LF determinations (see section 3.2), and black squares indicate our candidates. Fluxes with a detection significance below 1σ have been replaced with 1σ upper limits. Typical errorbars are shown in the upper right.

$$-0.5 < (UV_{275} - U_{336}) < 1.4 \quad \wedge \\ S/N(UV_{275}) > 5$$

This selects galaxies between $z \sim 1.3 - 1.7$, and results in 72 candidates down to $U_{336} = 26.5$.

Similarly, for UV_{275} -dropouts, the selection criteria are:

$$UV_{275} - U_{336} > 1 \quad \wedge \\ UV_{275} - U_{336} > 2.2(U_{336} - B_{435}) - 0.42 \quad \wedge \\ -0.5 < (U_{336} - B_{435}) < 1.1 \quad \wedge \\ S/N(U_{336}) > 5 \quad \wedge \quad S/N(UV_{225}) < 2$$

selecting galaxies between $z \sim 1.7 - 2.1$, with 131 candidates down to $B_{435} = 26.5$.

And finally, U_{336} -dropouts are selected with:

$$U_{336} - B_{435} > 1 \quad \wedge \\ U_{336} - B_{435} > 2(B_{435} - V_{606}) \quad \wedge \\ -0.5 < (B_{435} - V_{606}) < 1 \quad \wedge \\ S/N(B_{435}) > 5 \quad \wedge \quad S/N(UV_{225/275}) < 2$$

returning 434 sources down to $V_{606} = 26.5$ with expected redshifts in the range $z \sim 2.2 - 2.8$. When applying these criteria, all fluxes below their 1σ limits (in the dropout band) are replaced with the respective 1σ upper limits.

For the U_{336} -dropouts, the stellar sequence runs exactly through the selection window (see Figure 1). However, stars are removed prior to candidate selection using the same identification scheme as for the photo- z sample, resulting in a total of 40 excluded stars. From a final visual inspection of all sources no additional stars were found. A small number of clear diffraction spikes and spurious detections on the wings of large low-redshift galaxies were removed by hand.

Using our photometric redshifts, we estimate the low-redshift interloper fraction of these UV-dropout samples to be very small. In particular, only 7% of the sources in the U_{336} dropout sample have $z_{phot} < 1.75$. Similarly, only 4% and 8% of the sources in our UV_{275} - and UV_{225} -dropout samples are interlopers, i.e., have $z_{phot} < 1.25$ and $z_{phot} < 1$, respectively. Only sources down to the

limiting magnitudes of our UV LFs are considered in this estimate (see section 3.2).

3. RESULTS

3.1. Photometric Redshift LF Results

The UV luminosity functions at 1500 \AA in the range $z \sim 0.5 - 2$ are measured in three bins of photometric redshift of width $dz = 0.5$. The absolute magnitudes are computed from the UV_{275} , U_{336} and B_{435} photometry for sources in the redshift range $z = 0.5 - 1$, $z = 1 - 1.5$, and $z = 1.5 - 2$, respectively. K-corrections are derived from the appropriate best-fit templates.

The UV luminosity functions of galaxies are estimated using the standard V_{max} estimator (Schmidt 1968) such that

$$\phi(M)dM = \sum_i \frac{1}{C(m_i)V_{max,i}}$$

where the sum runs over all galaxies in the given redshift and absolute magnitude bin. We only include galaxies with $> 5\sigma$ detections in the corresponding filter, which results in the need for a completeness correction factor C . Following Oesch et al. (2007, 2010b), this is determined from Monte-Carlo simulations in which we add artificial galaxies to the images and detect them with the same SExtractor parameters as used for the original B-band catalog. The completeness is $> 97\%$ to ≤ 25 mag in the UVIS filters, after which it drops to 50% at 25.8 mag, which is our faint-end limit.

Figure 2 shows the resulting luminosity functions. The best-fit Schechter parameters (Schechter 1976) are tabulated in Table 1. While we sample the faint end rather well, with data that reaches ~ 2 mag fainter than M_* , the relatively small area covered by the ERS data results in some uncertainty on the cutoff at bright magnitudes. Nevertheless, our results are in good agreement with the LFs determined from GALEX by Arnouts et al. (2005) and effectively validate those results in data with ~ 50 times higher spatial resolution.

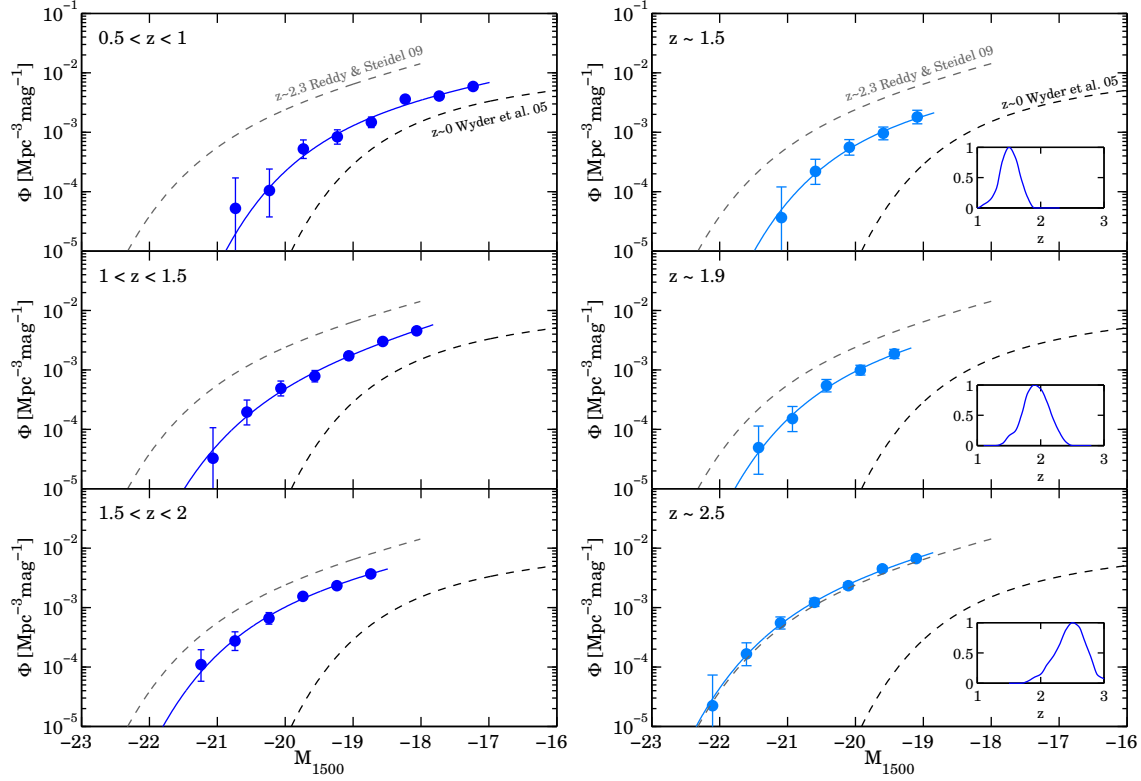


FIG. 2.— *Left*— The 1500 Å LF in the three different bins of photometric redshift. The blue data points with errorbars are the step-wise LFs determined with the V_{\max} method, and the solid blue lines represent our best-fit Schechter LFs to the step-wise LFs. The best-fit parameters are presented in Table 1. The black dashed line is the UV LF in the local universe from Wyder et al. (2005), while the gray dashed line is the UV LF between $z \sim 1.9 - 2.7$ from Reddy & Steidel (2009). *Right*— The 1500 Å LF derived from the LBG samples together with their best-fit Schechter LFs. From top to bottom: UV_{225-} , UV_{275-} , and U_{336} -dropout results. Again, the local $z \sim 0$ and the $z \sim 2.3$ LFs are shown for reference as black and gray dashed lines respectively. The insets show the expected redshift distributions of the dropout galaxies. This is estimated from the effective volumes and the best-fit Schechter LFs.

TABLE 1
UV LUMINOSITY FUNCTION PARAMETERS[†]

z	No. of Sources	$\log_{10} \phi_*$ [Mpc ⁻³ mag ⁻¹]	M_*	α
Photometric redshift samples				
0.5 – 1.0	284	-2.52 ± 0.31	-19.17 ± 0.51	-1.52 ± 0.25
1.0 – 1.5	284	-2.90 ± 0.25	-20.08 ± 0.36	-1.84 ± 0.15
1.5 – 2.0	288	-2.63 ± 0.23	-20.17 ± 0.34	-1.60 ± 0.21
UV-dropout samples				
1.5 ($\Delta z = 0.4$)	60	-2.64 ± 0.33	-19.82 ± 0.51	-1.46 ± 0.54
1.9 ($\Delta z = 0.4$)	99	-2.66 ± 0.36	-20.16 ± 0.52	-1.60 ± 0.51
2.5 ($\Delta z = 0.6$)	403	-2.49 ± 0.12	-20.69 ± 0.17	-1.73 ± 0.11

[†] Derived from χ^2 fits to the step-wise LFs.

3.2. Dropout LF Results

The UV LF of the UVIS dropout sample is computed using standard techniques adopted in LBG studies. In particular, the step-wise LFs are derived using

$$\phi(M[m_i, \bar{z}])dM = N_i/V_{\text{eff}}(m_i)$$

where N_i are the number of galaxies observed in the magnitude bin i , and the effective volume is given by:

$$V_{\text{eff}}(m_i) = \int_0^\infty S(m_i, z)C(m_i) \frac{dV}{dz} dz$$

The selection efficiency S and completeness C are again estimated from simulations of artificial galaxies inserted into the observed images. The inserted galaxies are chosen to have a log-normal size distribution, using an extrapolation of the higher redshift LBG size scaling of $(1+z)^{-1}$ (Oesch et al. 2010a; Bouwens et al. 2004; Ferguson et al. 2004). The colors are set according to the $z \sim 2.5$ UV continuum slopes derived in Bouwens et al. (2009) (see also Reddy et al. 2008), with additional IGM absorption according to Madau (1995).

Due to the lower sensitivity of the UV data with respect to the optical, red colors across the continuum

breaks cannot be accurately measured for galaxies fainter than $B \sim 26$. Therefore only sources with $V < 26.3$, $B < 25.5$, and $U_{336} < 25.4$ are used to compute the LFs, ensuring that the selection efficiency is still larger than 50% for U_{336} -, UV_{275} -, and UV_{225} -dropouts, respectively. This results in 403, 99, and 60 sources in the three different dropout samples.

The UV LFs for the UVIS dropouts are shown in the right panels of Figure 2. Again, a significant increase at the bright end of the UV LF is seen from lower to higher redshift. Due to the modest size of the present UV_{225} - and UV_{275} -dropout samples, the Schechter parameters we derive at $z \sim 1.5$ and $z \sim 1.9$ are still somewhat uncertain (see Table 1). The $z \sim 2.5$ U_{336} -dropout LF, by contrast, is much better constrained from our data, extending ~ 2 mag fainter than M_* and with a faint-end slope α established to within ± 0.11 . Our $z \sim 2.5$ LF is in excellent agreement with the $z \sim 2.3$ UV LF of Reddy & Steidel (2009).

Note that due to the limited area of the present survey, our results are dominated by cosmic variance, which we estimate to be about 16 – 20% (Trenti & Stiavelli 2008).

4. DISCUSSION

The evolution of the Schechter parameters of recent UV LFs in the redshift range $z \sim 0 - 8$ is shown in Figure 3. Our results cover the whole 4.3 Gyr period from $z \sim 0.75$ to $z \sim 2.5$. Interestingly, in the region of overlap, the LFs we derive from our photometric redshifts and UV dropout selections are in very good agreement. This suggests that our UV dropout samples are well-defined and reasonably complete.

In Figure 3, our results are compared to several Schechter function estimates from the literature. Within the uncertainties, ϕ_* is found to be fairly constant over the entire redshift range, although there is a weak trend towards higher ϕ_* at lower redshifts.

The most noteworthy trend is the monotonic fading of the characteristic luminosity by a factor of ~ 16 from $z \sim 3$ (M_* fades from -21 at $z \sim 3$ to -18 at $z \sim 0$). At $z > 4$, M_* turns over and decreases monotonically again towards higher redshift, such that $M_*(z = 8)$ is essentially equal to $M_*(z \sim 1)$.

It is very interesting that all our faint-end slope measurements are steeper than $\alpha \sim -1.5$, even at $z \sim 0.5 - 1$, in agreement with the earlier measurements of Arnouts et al. (2005). Despite relatively large errorbars, the faint-end slope α is clearly seen to transition from $\alpha < -1.5$ at $z \gtrsim 0.5 - 2$ to a flatter $\alpha = -1.2$ in the local universe (but see Treyer et al. 1998, who find a steeper slope locally). With the present data we cannot determine whether this transition occurs relatively abruptly at low redshift, or smoothly from $z \sim 2$ to $z \sim 0$.

Finally, in Figure 4 we show the cosmic 1500 \AA luminosity density ρ_L (uncorrected for dust extinction) estimated from the Schechter function parameters. The luminosity density is shown integrated to $L > 0.1L_{z=3}^*$ and also integrated to zero luminosity. Clearly, the evolution of ρ_L is mainly driven by M_* . From the peak at $z \sim 2.5$ the total UV luminosity drops by 1.5 dex to $z \sim 0$. This decrease is well described by $\rho_L(z) \propto (1+z)^{\beta_L}$, for which we find $\beta_L(z < 2.5) = 2.58 \pm 0.15$, in good agreement with earlier measurements (e.g. Schiminovich et al. 2005; Tresse et al. 2007). The evolution at higher redshift fol-

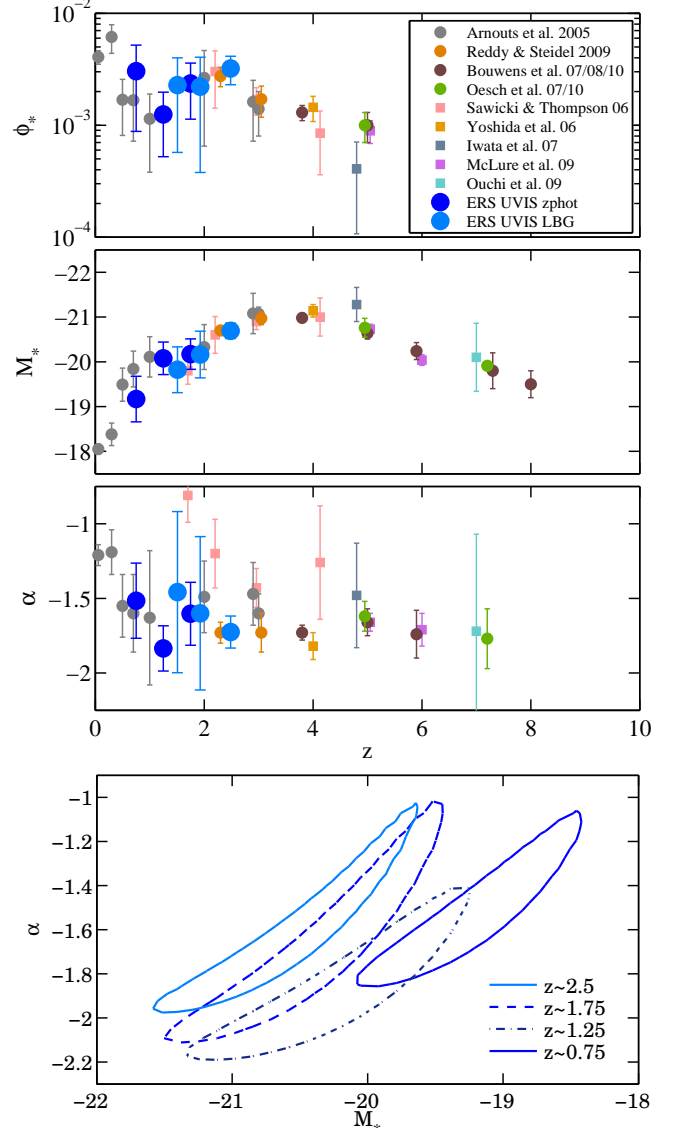


FIG. 3.— *Top Three Panels* — The redshift evolution of UV ($\lambda = 1500 - 1700 \text{ \AA}$) LF parameters ϕ_* , M_* , and α over the redshift range $z \sim 0 - 8$. The present determinations are shown with large filled circles. Of particular note, the uncertainties on the Schechter function parameters are frequently much smaller at $z > 3$ than at lower redshifts. This is a direct consequence of having very deep HST optical surveys. WFC3/UVIS should enable similarly-deep future observations in the UV at $z < 3$. Also shown are some notable determinations from the literature (Arnouts et al. 2005; Reddy & Steidel 2009; Bouwens et al. 2007, 2008; Bouwens et al. 2010; Oesch et al. 2007, 2010b; Sawicki & Thompson 2006; Yoshida et al. 2006; Iwata et al. 2007; McLure et al. 2009; Ouchi et al. 2009). Despite some scatter, most faint-end slope determinations at $z > 0.5$ are very steep, i.e. $\alpha \sim -1.7$. *Bottom* — The 68% error contours on M_* and α over the redshift range $z \sim 0.75 - 2.5$. The contour at $z \sim 2.5$ is from our U_{336} -dropout sample, the remaining ones are derived from the photometric redshifts. The lower redshift dropout samples result in considerably larger errors and are omitted for clarity.

lows $\beta_L(z > 2.5) = -1.82 \pm 0.37$. $z \sim 2.5$ thus marks the high point in the production of the cosmic UV luminosity and is clearly an important epoch for exploring the properties of galaxies (e.g. see Cameron et al. 2010, for a new technique for selecting galaxies in this range with simple color criteria).

The remarkable potential of the HST WFC3/UVIS

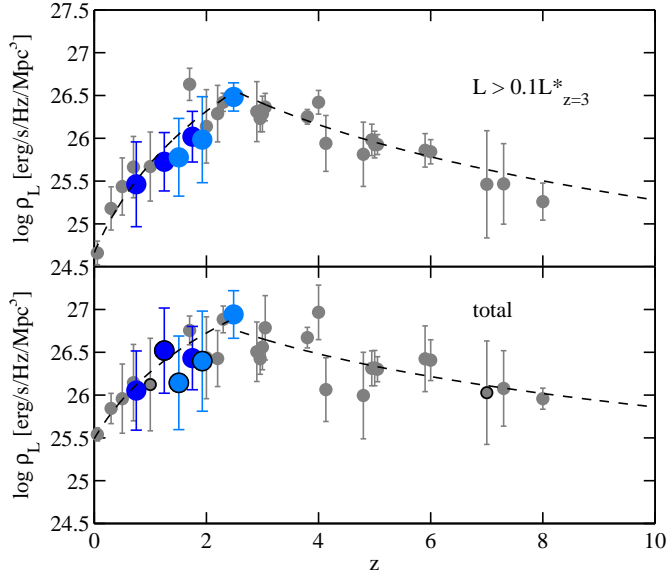


FIG. 4.— The redshift evolution of the UV ($\lambda \sim 1500 \text{ \AA}$) luminosity density. In the upper panel, the luminosity functions are integrated down to a fixed luminosity of $0.1L_{z=3}^*$ (L^* as derived at $z = 3$ by Steidel et al. 1999), while the lower panel shows the total luminosity density. The dark and light blue points are derived from our photo- z and the dropout samples respectively. The gray points are based on the literature values shown in Figure 3. The dashed curves are fits to the data at $z < 2.5$ and $z > 2.5$ of the form $\rho_L \propto (1+z)^{\beta_L}$. Errorbars are computed from Monte-Carlo simulations, not accounting for the covariance between the Schechter parameters. They are thus expected to overestimate the real errors. Note, however, that α was constrained to $\alpha > -2$ in order to keep ρ_L^{tot} finite. This only significantly affected 5 data points, which are marked with black circles.

camera is clear from these new results. This ERS dataset with its initial rather shallow observations has demonstrated already that WFC3/UVIS is a powerful tool for exploring galaxy evolution over the redshift range $z \sim 0.5$ to $z \sim 3$. Deeper data will provide key insights into the decline of the cosmic SFRD since $z \sim 2$, particularly at the lowest luminosities. For example, a steep LF with $\alpha \sim -1.7$ suggests that star-formation efficiencies and feedback processes are only weakly dependent on halo mass (e.g. Trenti et al. 2010).

We thank the GOODS and the GOODS-MUSIC teams for providing their data to the community. PO acknowledges support from the Swiss National Foundation (SNF). This work has been supported by NASA grant NAG5-7697 and NASA grant HST-GO-11563.

Facilities: HST(ACS/WFC3), VLT(ISAAC), VLT(VIMOS), Spitzer(IRAC).

REFERENCES

- Arnouts, S., et al. 2005, *ApJ*, 619, L43
 Bertin, E., & Arnouts, S. 1996, *A&AS*, 117, 393
 Bouwens, R. J., et al. 2004, *ApJ*, 611, L1
 —. 2007 *ApJ*, 670, 928
 —. 2008, *ApJ*, 686, 230
 —. 2009, *ApJ*, 705, 936
 —. 2010, *ApJ*, 709, L133
 Bruzual, G., & Charlot, S. 2003, *MNRAS*, 344, 1000
 Budavári, T., et al. 2005, *ApJ*, 619, L31
 Bunker, A. J., et al. 2010, *MNRAS*, 409, 855
 Burgarella, D., et al. 2006, *A&A*, 450, 69
 Capak, P., et al. 2007, *ApJS*, 172, 99
 Calzetti, D., et al. 2000, *ApJ*, 533, 682
 Cameron, E., et al. 2010, *arXiv:1007.2422*
 Coleman, G. D., et al. 1980, *ApJS*, 43, 393
 Feldmann, R., et al. 2006, *MNRAS*, 372, 565
 Ferguson, H. C., et al. 2004, *ApJ*, 600, L107
 Giavalisco, M., et al. 2004, *ApJ*, 600, L93
 Habertzettl, L., et al. 2009, *ApJ*, 702, 506
 Hathi, N. P., et al. 2010, *ApJ*, 720, 1708
 Iwata, I., et al. 2007, *MNRAS*, 376, 1557
 Kennicutt, Jr., R. C. 1998, *ARA&A*, 36, 189
 Lilly, S. J., et al. 2007, *ApJS*, 172, 70
 Lilly, S. J., et al. 2009, *ApJS*, 184, 218
 Ly, C., et al. 2009, *ApJ*, 697, 1410
 Madau, P. 1995, *ApJ*, 441, 18
 McLure, R. J., et al. 2009, *MNRAS*, 395, 2196
 —. 2010, *MNRAS*, 403, 960
 Oesch, P. A., et al. 2007, *ApJ*, 671, 1212
 —. 2010a, *ApJ*, 709, L21
 —. 2010b, *ApJ*, 709, L16
 Oke, J. B., & Gunn, J. E. 1983, *ApJ*, 266, 713
 Ouchi, M., et al. 2009, *ApJ*, 706, 1136
 Pickles, A. J. 1998, *PASP*, 110, 863
 Reddy, N. A., & Steidel, C. C. 2009, *ApJ*, 692, 778
 Reddy, N. A., et al. 2008, *ApJS*, 175, 48
 Santini, P., et al. 2009, *A&A*, 504, 751
 Sawicki, M., & Thompson, D. 2006, *ApJ*, 642, 653
 Schechter, P. 1976, *ApJ*, 203, 297
 Schiminovich, D., et al. 2005, *ApJ*, 619, L47
 Schmidt, M. 1968, *ApJ*, 151, 393
 Steidel, C. C. et al. 1995, *AJ*, 110, 2519
 Steidel, C. C., et al. 1999, *ApJ*, 519, 1
 Trenti, M., & Stiavelli, M. 2008, *ApJ*, 676, 767
 Trenti, M., et al. 2010, *ApJ*, 714, 202L
 Tresse, L., et al. 2007, *A&A*, 472, 403
 Treyer, M. A., et al. 1998, *MNRAS*, 300, 303
 Windhorst, R. et al. 2010, *arXiv:1005.2776*
 Wyder, T. K., et al. 2005, *ApJ*, 619, L15
 Yoshida, M., et al. 2006, *ApJ*, 653, 988